

Solubility equilibria: From chemical potentiometry to industrial applications

Heinz Gamsjäger

Abteilung für Physikalische Chemie, Montanuniversität Leoben,
Franz-Josef-Strasse 18, A-8700 Leoben, Austria

Abstract

Solubility equilibria are related to thermodynamic properties in general and chemical potentials in particular of ionic compounds, nonelectrolytes and metals in aqueous solutions or melts. Solubility phenomena are most efficiently dealt with by the theoretical and graphical methods of phase theory. Master variables for the depiction of the pertinent solid-solid or solid-liquid phase diagrams are deduced from generalized Gibbs-Duhem equations. Solubility techniques in aqueous media contribute to information on thermodynamic quantities of sparingly as well as highly soluble ionic compounds, which may play a role in geochemistry and/or industry. For solving multiphase multicomponent equilibrium problems in this context the general Gibbs energy minimizing program ChemSage was used together with a new optimization routine.

At the temperatures of aqueous solutions solid-solid phase transformations and/or recrystallizations are often much slower than equilibration between solid and liquid phases. It is shown that thermodynamically reliable data from dissolution studies on metastable systems can be obtained.

Finally the role of solubility phenomena in physical metallurgy is addressed. An example for the application of solubility information to an industrial problem is presented.

Introduction

In aqueous solutions a well established method of chemical potentiometry in the sense of McGlashan [1] is based on the measurement of freezing point depression data. Clearly at the freezing point a solution is saturated with respect to the solvent, and in perfect analogy the solubility is determined by saturation with respect to the solute. Consequently, in principle solubility and freezing point data can be interpreted by the same thermodynamic formalism. Regardless of the well known practical limitations on cryoscopic and solubility methods [1, 2] research activities employing the latter have been revived recently [3]. Two reasons for this renewed interest are quite obvious, a) versatile computer programs exist which simultaneously use solubility, isopiestic, potentiometric and calorimetric data for parameter optimization of the thermodynamic model under investigation, b) solubility phenomena in itself are of practical importance in geochemistry as well as chemical and metallurgical industry [4].

The first part of this paper is somewhat tutorial in character and emphasizes the efficiency of phase diagrams to describe the solubility behaviour of electrolytes, nonelectrolytes and metals. It should be pointed out that recently many practical aspects of phase behaviour have been vividly summarized on an elementary level [5, 6].

The second part deals with information obtained from studies of different types of metastable equilibria between solids and aqueous solutions from which reliable thermodynamic quantities can be derived, although only a local and not the global minimum of the relevant Gibbs function is attained. The role of "stoichiometric saturation" [7] in this context has been clarified only recently [8–13].

In the last part a digression on solubility phenomena in metallurgy seems justified, because in this field phase theory is highly developed and a fruitful feedback to chemistry is to be expected. Thus, several concepts being discussed in the present paper originated from metallurgy oriented research activities. The topological principle of phase diagrams [14], the consistency test based on the slopes of phase boundaries [15], and the Unified Interaction Parameter Formalism [16] may serve as examples.

Thermodynamic Significance of Solubilities

The common basis of phase diagrams are generalized Gibbs-Duhem equations (1)

$$X_{m,1} dY_1 + X_{m,2} dY_2 + X_{m,3} dY_3 + \dots + X_{m,c} dY_c = 0 \quad (1)$$

where the generalized potentials $Y_i (T, -p, \mu_i)$ must have the same value in all parts of the system [14]. When all conjugate molar quantities $X_{m,i} (S_m, V_m, x_i)$ are defined in the same way, i.e. with the same definition of the amount n [17], the phase behaviour in general and the solubility in particular is best represented by two-dimensional diagrams of three different types depending on the choice of the variables (I: $Y_j - Y_k$, II: $Y_j - X_{m,k}$ or $X_{m,j} - Y_k$, III: $X_{m,j} - X_{m,k}$). Potential diagrams (I) and the two kinds of molar phase diagrams (II, III) are topologically distinguishable. For the coexistence of two phases α and β in a binary system of components A, B two equations of type (1) must be satisfied simultaneously. Rearrangement in terms of the variables T, p, x^α and T, p, x^β leads to equation (2) or its analogue, sometimes either called Gibbs-Konovalov [1] or Van der Waals equations [18].

$$\left\{ (1 - x^\beta) \Delta_\alpha^\beta H_A + x^\beta \Delta_\alpha^\beta H_B \right\} d \ln T - \Delta_\alpha^\beta V_m dp + (x^\beta - x^\alpha) \left(\partial^2 G_m / \partial x^2 \right)_{T,p}^\alpha dx^\alpha = 0 \quad (2)$$

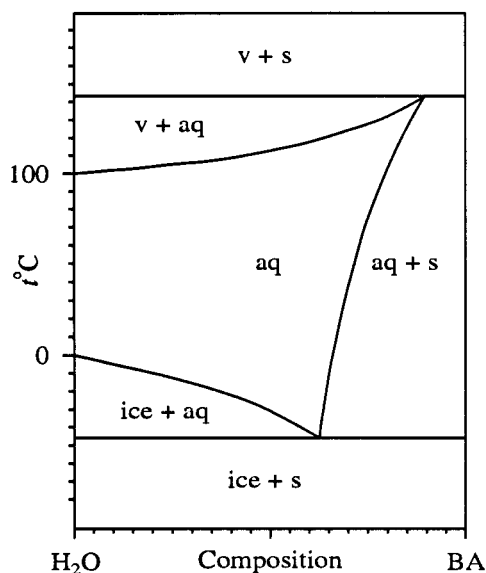


Fig. 1 General aqueous phase diagram.
v: Vapour, s: Solid BA, aq: Aqueous solution.

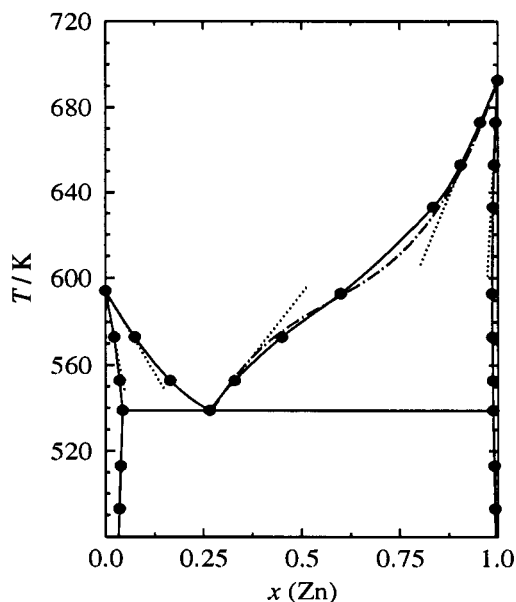


Fig. 2 Phase diagram Cd - Zn.
Solid curves and •: Optimized diagram,
dot-dashed curve: Simplified subreg. model,
dotted lines: Slopes at phase boundaries.

General Aqueous Phase Diagram

Let us imagine a simple system made up of water and a solid ionic compound BA. At constant

pressure of say 1 bar the most versatile molar (T, x) phase diagram of Fig. 1 consists of three intersecting boiling point, freezing point and solubility curves. The properties of two actually coexisting phases are related by type (2) equations. Thus, the temperature of solid – aqueous solution separation, the so called solutus (a more general term is liquidus), can be calculated from the corresponding thermodynamic properties and vice versa. Two horizontal three-phase equilibrium lines enclose the stability field of solutions.

Phase Diagram of the Cd – Zn System

Aqueous and metallic diagrams differ conspicuously in two aspects, namely ionic compounds are in general not soluble in ice, whereas many alloys exhibit a more or less extended solid solubility. Furthermore, the boiling point of water is far below the melting points of most ionic compounds, whereas rarely one metal component evaporates while the other has not even melted. Recently the Cd-Zn phase diagram has been optimized [19], see Fig. 2. It should be emphasized that a subregular model neglecting the solid solubility of cadmium in zinc reproduces the zinc-rich liquidus good enough for many practical purposes. For invariants of binary systems (A, B) at three phase equilibria (α, β, γ) – like the eutectic – equation (3) relates the ratio of the slopes at the phase boundaries with thermodynamic quantities. When various approximations apply, only the entropies of fusion of the pure components and the composition of the invariant will be needed to predict these ratios.

$$\frac{(\partial T/\partial x)_{\gamma+\beta}}{(\partial T/\partial x)_{\gamma+\alpha}} = \frac{[(1-x^\alpha)\Delta_\alpha^\gamma S_A + x^\alpha\Delta_\alpha^\gamma S_B](x^\beta - x^\gamma)}{[(1-x^\beta)\Delta_\beta^\gamma S_A + x^\beta\Delta_\beta^\gamma S_B](x^\alpha - x^\gamma)} \quad (3)$$

Although many excellent programs for computer assisted calculation and optimization of phase diagrams are available, the general slope test at invariant points still serves as a quick check on the consistency of phase diagrams [15]. Even the simplified liquidus on the Zn-rich side passes the test.

Phase Diagram of the Water – Urea System

The water – ionic compound and water – urea diagrams differ because the melting point of urea is much lower than that of most inorganic ionic compounds, thus the distinction between solvent and solute becomes arbitrary and in fact the latter system can be treated symmetrically. Using molality (m) as composition variable the water-urea diagram shown in Fig. 3 has been plotted with solubility data measured by a 94 class of undergraduate students. Although the temperature range is narrow and the data were fitted to a simple one parameter excess Gibbs function model, the predicted solubility curve is close to that deduced from published data. As the differential enthalpy of solution at saturation is difficult to measure calorimetrically [23] the Williamson equation (4) is often used instead [24]. Again the 25°C values of the solubility and its temperature derivative obtained by undergraduates agree satisfactorily with accepted data.

$$\Delta_{\text{sol}}H/RT^2 = (dm/dT)_{\text{sat}} [(\phi/m)_{\text{sat}} + (\partial\phi/\partial m)_{\text{sat}}] \quad (\phi : \text{osmotic coefficient}) \quad (4)$$

The same types of diagram depict the phase behaviour of sparingly soluble compounds, however, it may be expedient to plot temperature versus logarithms of composition variables.

Gibbs-Duhem Equation for Solid-Solution Aqueous Solution Equilibria

Let us now consider ternary aqueous systems with two 1:1 ionic compounds (BA, CA) having a common anion and no water in the solid phase. The generalized Gibbs-Duhem equations (1) for solid-solution (5) aqueous-solution (6 or 7) equilibria at constant temperature and pressure are now given by:

$$(1 - x^s) d \ln a_{\text{BA}} + x^s d \ln a_{\text{CA}} = 0 \quad (5)$$

$$(1 - x^{\text{aq}}) d \ln a_{\text{BA}} + x^{\text{aq}} d \ln a_{\text{CA}} + (1/M_{\text{H}_2\text{O}} \Sigma m) d \ln a_{\text{H}_2\text{O}} = 0 \quad (6)$$

$$(1 - x^{\text{aq}}) d \ln (\{B^+\}\{A^-\}) + x^{\text{aq}} d \ln (\{C^+\}\{A^-\}) - (2/\Sigma m) d(\phi \Sigma m) = 0 \quad (7)$$

As an example the respective phase diagrams of the system KBr-KI-H₂O are depicted in Fig. 4.

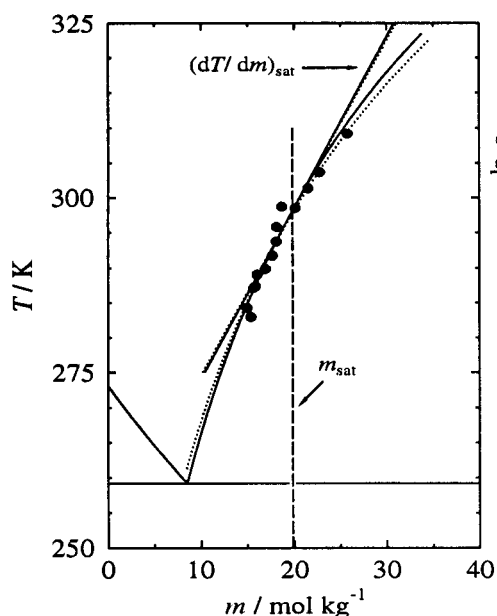


Fig. 3 Solubility of urea in water. Solid curves and lines: Calc. reg. model, dotted curve and line: Calc. subreg. model, ● exp. data (undergraduate lab).

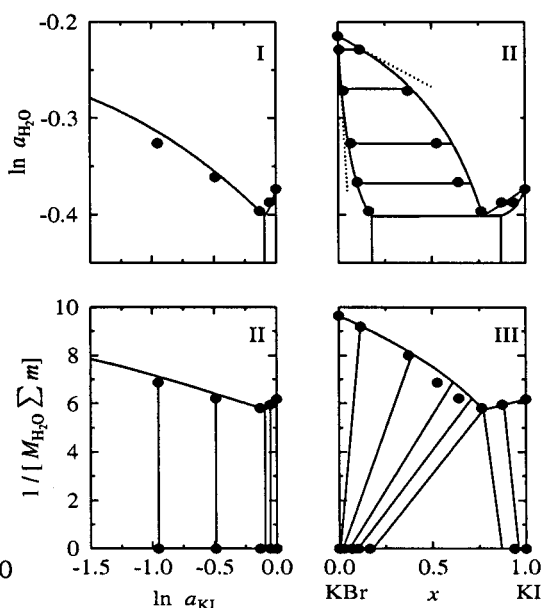


Fig. 4 Phase diagrams of KBr-KI- H₂O. At 25°C, Types I, II, III, ● exp. data [20], solid curves and lines: Calc. [21, 22].

By plotting $\ln a_{\text{H}_2\text{O}}$ or the osmotic coefficient times the molality sum $\Sigma m = m_{\text{KBr}} + m_{\text{KI}}$ versus the mole fraction coordinate, type II diagrams topologically equivalent to the familiar T, x diagrams are obtained [25]. It is noted in passing that the ratio of the limiting solidus and solutus slopes at $x_{\text{KI}} = 0$ equals the ideal distribution coefficient x^s/x^{aq} provided the phase diagram is thermodynamically consistent.

When $\phi = 1$ and $d\phi = 0$ the Gibbs-Duhem equation (7) for the aqueous phase simplifies to

$$(1 - x^{\text{aq}}) d \ln ([\text{B}^+][\text{A}^-]) + x^{\text{aq}} d \ln ([\text{C}^+][\text{A}^-]) - d \ln (\Sigma m)^2 = 0 \quad (8)$$

and with $(\Sigma m)^2 = \Sigma K$, Lippmann $\ln \Sigma K - x$ diagrams equivalent to true phase diagrams ensue (see Fig. 5). Some years ago Lippmann proposed to plot the total solubility variable versus the activity fraction [26]. Both types of diagrams become equivalent when $\phi = 1$.

Plotting the potential variable $\phi \Sigma m$ versus the molar variable x leads in any case to thermodynamically consistent diagrams, whereas for highly soluble salts the activity fraction x^{act} used by Lippmann [26] cannot correctly predict invariants like the “quasi eutectic” in Fig. 4, because x^{aq} not necessarily equals x^{act} .

Finally, inspection of Fig. 4 reveals that $\ln a_{\text{H}_2\text{O}}$, $\ln a_{\text{KI}}$ and $1/M_{\text{H}_2\text{O}} \Sigma m$, x_{KI} diagrams belong to type I and III respectively. The latter corresponds to the often used Jänecke [27] diagrams.

Throughout this work binary and, the more so, higher phase diagrams have been calculated with the general Gibbs energy minimizing program ChemSage [28], which is capable of simultaneously solving multiphase multicomponent equilibrium problems in open or closed systems. ChemSage has become even more versatile since an optimization routine had been incorporated [29]. Thereby standard Gibbs energies and excess Gibbs functions can be optimized with regard to experimental data originating from phase equilibria, activities, and potentiometric or calorimetric measurements.

Recently activity coefficients of salts forming binary solid solutions and differing with respect to only one ion, were derived solely on the basis of careful solubility measurements [30]. This was achieved under the simplifying assumption of equal activity coefficients of the exchanging ions in the aqueous phase. The merits of this straightforward method are indisputable, however, in the present context the intention was to use as many independent experimental data as possible for the calculation of the relevant thermodynamic quantities.

Thermodynamic Quantities from Metastable Equilibria

Phase Diagram of Mg-Calcites

When metastable equilibria are considered the phase behaviour of the calcite–magnesite–water system can be re-interpreted. Application of the Unified Interaction Parameter Formalism reconciles the apparently contradictory experimental results [16, 31]. In the pertinent case reference states have been selected so that magnesian calcites can be regarded in a Henrian sense as dilute solutions of MgCO_3 in the solvent CaCO_3 . The respective Lippmann diagram is shown in Fig. 5.

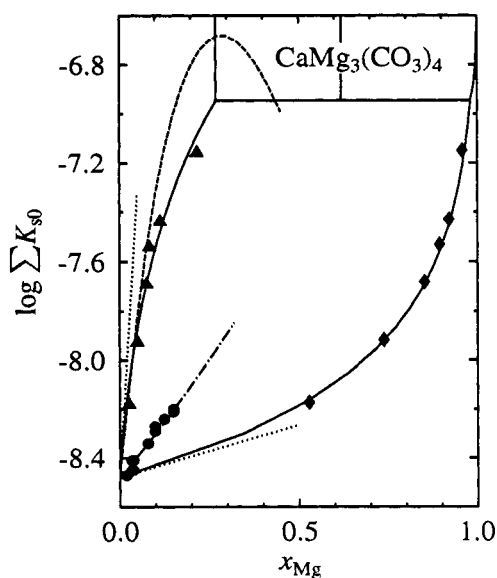


Fig. 5 Phase diagram of Mg-calcites. Solid curves and lines: Calc. UIPF [16, 31], dashed curve: Calc. endmember magnesite, dotted lines: Limiting slopes at phase boundaries, dot-dashed line: Equal G -curve, ● exp. data [32, 33], Δ solidus, ◇ solutus data [34].

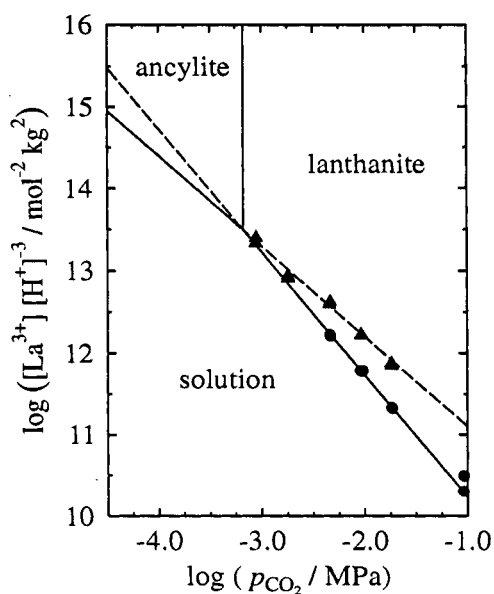


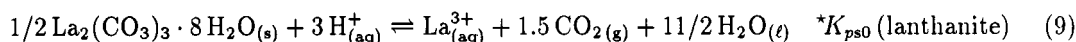
Fig. 6 Predominance diagram of La-carbonates. At 25°C , $I = 0.1 \text{ mol kg}^{-1}$ ● exp. data lanthanite, Δ exp. data ancyllite, solid lines: Stable range, dashed lines: Metastable range.

Careful experiments resulted in congruent dissolution of magnesian calcites [32, 33], a phenomenon termed “stoichiometric saturation” [7], which has been shown to be a constrained metastable equilibrium [8, 9]. Stoichiometric saturation states are characterized by equal G -functions of both solid and solution phases. If magnesite, or dolomite, are employed as endmembers for modelling the magnesian calcite solid-solutions, the results obtained from dissolution experiments [32, 33] suggest a large, positive excess Gibbs function which predicts an extensive region of demixing. Precipitation of solid-solutions, containing up to 20 mol-% MgCO_3 , in (metastable) equilibrium with aqueous solutions should be impossible. However, just this has been unequivocally proved by very careful precipitation experiments [34]. The precipitation of dolomite and magnesite from aqueous

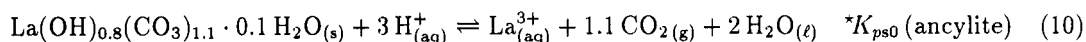
solution is kinetically inhibited at ambient temperature and pressure. Thus, it is suggested to dispense with models, which regard dolomite or magnesite as endmembers of the magnesian calcites in solid-solution aqueous-solution equilibria. In Fig. 5 metastable states are taken into account and the phase behaviour of magnesian-calcites is predicted correctly. It should be emphasized, however, that the Unified Interaction Parameter Formalism is only applicable for comparatively dilute solutions. Consequently, a pure MgCO_3 -phase which would be several orders of magnitude more soluble than magnesite is physically meaningless.

Solubility of Lanthanum Carbonates

Recently in our laboratory the solubility constants of lanthanite, $\text{La}_2(\text{CO}_3)_3 \cdot 8 \text{H}_2\text{O}$, according to equation (9) were determined at varying ionic strengths in order to obtain an accurate value of its Gibbs energy of formation [35].



This can be achieved by combining the “thermodynamic” solubility constant and the La^{3+}/La standard electrode potential values at infinite dilution with well-established thermodynamic quantities. Solubility constants for unspecified lanthanum carbonates given in the literature are ca. 10 and 500 times respectively, higher than the mean value found in our study [36, 37]. Such discrepancies can usually only be explained, when different solid substances have been investigated. In fact a basic lanthanum carbonate, ancylite ($\text{La}(\text{OH})_{0.8}(\text{CO}_3)_{1.1} \cdot 0.1 \text{H}_2\text{O}$), can be prepared similar to lanthanite by precipitation from solution. For ancylite the molar ratio of $\text{La}:\text{OH}:\text{CO}_3$ varies from 1:0.6:1.2 to 1:1:1 according to different authors [38, 39]. In addition to chemical and thermogravimetric analyses the formula of ancylite was ascertained by solubility measurements at varying p_{CO_2} and pH. The solubility constant of ancylite according to equation (10) was indeed found to be ca. one order of magnitude higher than that of lanthanite.



From these studies it can be concluded that: 1) The Pitzer equations are useful to extrapolate solubility constants ${}^*K_{ps0}^I$ to zero ionic strength, particularly in simple cases where only one species as e.g. the aqua ion controls the overall solubility of the metal. 2) ${}^*K_{ps0}^0$ values thus obtained lead to accurate Gibbs energies of formation. 3) Measurements carried out in a constant ionic medium may be used to calculate the respective value of the solubility at infinite dilution provided the ionic strength is not higher than ca. 1 mol kg^{-1} . 4) The ternary Pitzer parameters needed to predict solubilities at higher ionic strengths have still to be optimized. Once this has been achieved a wealth of already existing experimental information can be made to contribute to thermodynamic data banks.

The predominance area diagram in Fig. 6 shows paradigmatically the efficiency of thermodynamics under favourable conditions. All data on ancylite leading to its standard Gibbs function have been obtained in its metastable range. Moreover, guided by Fig. 6 a procedure for preparing ancylite was developed, and indeed beautifully pure crystals of this substance have thus been obtained.

Solubility Phenomena and Metallurgy

Solubilities of metals in solid and liquid phases are of interest in extractive as well as physical metallurgy. An application in the latter field is discussed in the concluding paragraph.

Computer Assisted Optimization of Cobalt-Base Alloy Compositions

Cobalt-base hard metals consisting of Co-Cr-W-C are known for their wear and corrosion resistance, and also for their ability to retain hardness at elevated temperatures. These alloys are either produced as castings or as sintered parts. To locate ranges for optimal matrix and carbide compositions of sintered products thermodynamic calculations with ChemSage [28] were carried out on

the basis of recently published data which were improved by the new optimization routine [29, 40]. Considering the properties of these alloys it can be predicted that a) the performance against corrosive media will improve when the Cr content is increased, care has to be taken in the course of liquid-phase sintering to avoid b) unwished-for carbides and/or c) intermetallic phases, because these would be detrimental with respect to mechanical properties of the alloys, d) a higher W content will turn out advantageous because of its solid-solution strengthening effect.

In Fig. 7 the projection of a solidus surface is shown for a commercially available alloy with 1.15 wt-% C (●). The ranges of total Cr and W content are chosen so as to show the existence fields of the following phase combinations (carbides symbolized by their formula): a) *fcc* (matrix) + M_7C_3 ; b) *fcc* + M_7C_3 + $M_{23}C_6$; c) *fcc* + $M_{23}C_6$. Those fields, where additional phases become stable, are labeled with + in front of the phase symbol. Now the compositional range can be selected so that chromium carbides as hardening phases are formed and tungsten carbides are avoided. Moreover, for each of the three phase combinations a), b), and c), that range can be chosen with the maximum Cr and an acceptable W content.

Conclusions regarding the above mentioned expected effects can be drawn from Fig. 8, which shows the solubilities of Cr and W in the matrix for two series of alloys at 11 (A) and 8 wt-% W (B): As expected, Cr dissolved in the matrix increases monotonically with total Cr, and levels off in the existence field of *fcc* + M_7C_3 + $M_{23}C_6$. Likewise, the solubility of W in the matrix remains almost constant and drops noticeably when $M_{23}C_6$ becomes stable. Thus, solidus surface projections reveal that a higher Cr content in the matrix can be obtained with alloy series B, while a W content of 8 wt-% presumably still suffices for solid-solution strengthening. In addition, Fig. 8 shows calculated (T_{solidus} ●) and experimental (T_{ambient} ◇) results for a commercial alloy (Co-28Cr-4W-1.15C) which agree amazingly well, although they refer to differing temperatures, cf [41].

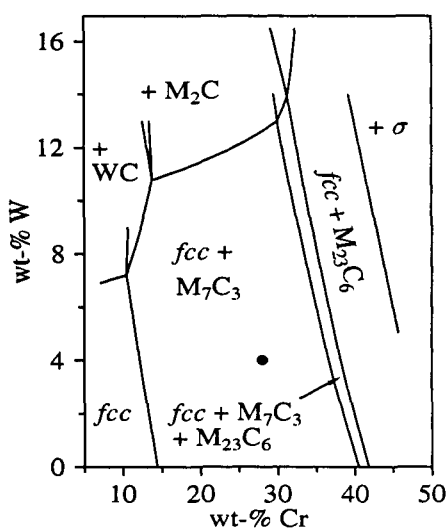


Fig. 7 Projection of solidus surface.
Meaning of symbols: See text.

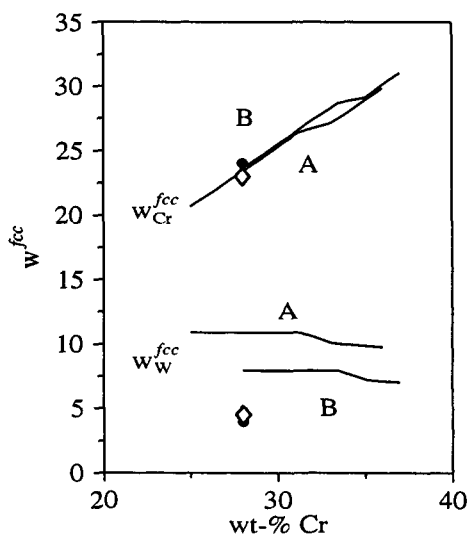


Fig. 8 Cr and W content of *fcc* matrix.
Meaning of symbols: See text.

Acknowledgements

Financial support by the Austrian Science Foundation (Project 8120-CHE) and an additional travel fund of the Österreichische Forschungsgemeinschaft are gratefully acknowledged.

References

- [1] M.L. McGlashan, *Chemical Thermodynamics*, Academic Press, London (1979).
- [2] G.N. Lewis and M. Randall, revised by K.S. Pitzer and L. Brewer, *Thermodynamics*, McGraw-Hill, New York (1961).
- [3] R.T. Pabalan and K.S. Pitzer, *Mineral solubilities in electrolyte solutions*, in K.S. Pitzer, editor, *Activity coefficients in electrolyte solutions*, p.435, CRC Press, Boca Raton, Florida, (1991).
- [4] H. Gamsjäger. *Aquatic Sciences* **55**, 314 (1993).
- [5] R.G. Laughlin. *J. Chem. Educ.* **69**, 26 (1992).
- [6] R.S. Treptow. *J. Chem. Educ.* **70**, 616 (1993).
- [7] D.C. Thorstenson and L.N. Plummer. *Am. J. Sci.* **277**, 1203 (1977).
- [8] H. Gamsjäger. *Ber. Bunsenges. Phys. Chem.* **89**, 1318 (1985).
- [9] E. Königsberger and H. Gamsjäger. *Ber. Bunsenges. Phys. Chem.* **91**, 785 (1987).
- [10] P.D. Glynn and E.J. Reardon. *Am. J. Sci.* **290**, 164 (1990).
- [11] P.D. Glynn *et al.* *Geochim. Cosmochim. Acta* **54**, 267 (1990).
- [12] E. Königsberger and H. Gamsjäger. *Am. J. Sci.* **292**, 199 (1992).
- [13] P.D. Glynn and E.J. Reardon. *Amer. J. Sci.* **292**, 215 (1992).
- [14] H. Schmalzried and A.D. Pelton. *Ber. Bunsenges. Phys. Chem.* **77**, 90 (1973).
- [15] A.D. Pelton. *Met. Trans. A* **19A**, 1819 (1988).
- [16] C.W. Bale and A.D. Pelton. *Metall. Trans. A* **21 A**, 1997 (1990).
- [17] M. Hillert. *International Metals Reviews* **30**, 45 (1985).
- [18] H.A.J. Oonk, *Phase Theory*, Elsevier Scientific Publishing Company, Amsterdam (1981).
- [19] S.C. Choi. *CALPHAD* **14**, 307 (1990).
- [20] L.L. Makarov and K.K. Evstrop'ev. *Russ. J. Phys. Chem.* **34**, 934 (1960).
- [21] K.S. Pitzer. *J. Phys. Chem.* **77**, 268 (1973).
- [22] E. Königsberger. *Monatsh. Chem.* **121**, 999 (1990).
- [23] H.-H. Emons *et al.* *Thermochim. Acta* **81**, 59 (1984); **104**, 139 (1986); **104**, 147 (1984).
- [24] A.T. Williamson. *Trans. Faraday Soc.* **40**, 421 (1944).
- [25] E. Königsberger and H. Gamsjäger. *Ber. Bunsenges. Phys. Chem.* **95**, 734 (1991).
- [26] F. Lippmann. *N. Jb. Miner. Abh.* **139**, 1 (1980).
- [27] E. Jänecke. *Z. Anorg. Chem.* **51**, 132 (1906).
- [28] G. Eriksson and K. Hack. *Metall. Trans. B* **21 B**, 1013 (1990).
- [29] E. Königsberger and G. Eriksson. *CALPHAD* (1994). Submitted for publication.
- [30] N.O. Smith. *J. Solution Chem.* **21**, 1151 (1992); **23**, 521 (1993).
- [31] E. Königsberger and H. Gamsjäger. *Geochim. Cosmochim. Acta* **56**, 4095 (1992).
- [32] W.D. Bischoff *et al.* *Geochim. Cosmochim. Acta* **51**, 1413 (1987).
- [33] E. Busenberg and L.N. Plummer. *Geochim. Cosmochim. Acta* **53**, 1189 (1989).
- [34] A. Mucci and J.W. Morse. *Geochim. Cosmochim. Acta* **47**, 217 (1983).
- [35] A.M. Nguyen *et al.* *Monatsh. Chem.* **124**, 1011 (1993).
- [36] N. Jordanov and I. Havezov. *Z. anorg. allg. Chem.* **347**, 101 (1966).
- [37] F.H. Firsching and J. Mohammadzadel. *J. Chem. Eng. Data* **31**, 40 (1986).
- [38] M. Akinc and D. Sordelet. *Advanced Ceramic Materials* **2**, 232 (1987).
- [39] L. Moscardini d'Assunção *et al.* *Thermochim. Acta* **137**, 319 (1989).
- [40] P. Waldner *et al.* *J. Alloys Comp.* **193** (1994). Accepted for publication.
- [41] K.C. Antony. *Journal of Metals* **35**, 52 (1983).